Error Statistics of 64-QAM Signal in AM/64-QAM Hybrid Optical Transmission

Kazuki Maeda, *Member, IEEE*, and Shozo Komaki, *Senior Member, IEEE*

***Abstract*—This paper describes the performance of an error correction system based on the DAVIC specifications. It also presents an error statistics property and its analytical model for the impulse noise induced by clipping in amplitude modulation (AM)/64 quadrature amplitude modulation (QAM) hybrid optical transmission (hybrid transmission). We found in hybrid transmission that the errors cannot be completely corrected by the error correction of DAVIC after bit error rate (BER) measurement with error correction, and then the error statistics of the 64-QAM channel were evaluated. It was confirmed that errors occasionally occur in long bursts that exceed an interleaver block length of the error correction when the impulse noise degrades the 64-QAM signal's BER. We believe that the error burst is caused by the slowed fluctuation of the envelope of a frequency division multiplex (FDM) signal in hybrid transmission. Once a portion of the envelope amplitude reaches the clipping level, the duration of maintaining such a condition is much longer than the 64-QAM symbol time. Accordingly, the errors occasionally run for more than 100 symbols. We apply Rice's fading duration distribution model to explain this error burst occurrence mechanism and its statistical manner and discuss this model's validity by comparison between the theoretical and measurement data of error statistics property. Consequently, we found that the theoretical value by the proposed model is in excellent agreement with the measurement data and confirmed that the proposed model is valid for analyzing the error manner for the clipping induced error.**

***Index Terms*—Cable television (CATV), error analysis, impulse noise, quadrature amplitude modulation (QAM), subcarrier multiplexing (SCM).**

I. Introduction

IT is widely recognized that future cable television (CATV) systems will require additional channel capacity for digital video transmission to incorporate new services such as video-on-demand. A hybrid fiber and coaxial (HFC) system using an analog/digital hybrid optical transmission technique (hybrid transmission) is expected to satisfy such requirements. However, in hybrid transmission, the quadrature amplitude modulation (QAM) signal's bit error rate (BER) is degraded by an impulse noise due to clipping in a laser diode; furthermore, the BER exhibits a "floor-like" manner even if hybrid transmission achieves high-quality amplitude modulation (AM) video signal transmission [1], [2].

In hybrid transmission, the AM signal's optical modulation index (OMI) should be set as large as possible without the distortion levels exceeding the required value to achieve the best carrier-to-noise ratio (CNR) for the AM signals. Thus, clipping is an inevitable phenomenon, and since the BER degradation due to impulse noise is assumed in advance, the required BER should be obtained by only using the proper error correction in HFC systems. In the DAVIC specification [3], on the other hand, an error correction for digital modulation signals in CATV systems is provided. The recommended error correction of DAVIC for 64-QAM signal transmission employs the (204, 188) Reed–Solomon code and convolutional interleaving with a depth of 12. This seems to be a powerful enough error correction, but we believe that more careful discussion is necessary to select the best error correction in CATV systems with HFC because the errors caused by impulse noise show a distinct burst-like behavior [4]. Previous studies discussed density of the clipping occurrence and averaged clipped duration of the FDM signal [5]–[7]. These results, however, do not give a clear explanation of the error burst that would be caused by the series of clipping occurrences. Furthermore, the performance of the DAVIC recommended error correction under the impulse noise condition had been reported [7], [8], and the effect of an interleaver depth on errors in the hybrid systems had been discussed [9]. Such discussions have suggested that we need to consider these burst errors for designing error correction to realize high quality transmission for digital signals in the HFC systems. Previous papers suggested that the DAVIC recommended error correction is not always effective for errors induced by clipping.

The remainder of this paper is organized as follows. Section II presents an error occurrence mechanism and an error statistics model of the 64-QAM signal in hybrid transmission. Section III describes measurement results of error correction performance and the error occurrence manner of impulse noise. In Section IV, we compare the analysis results by the proposed model and measurement results and demonstrate the validity of the proposed model for evaluating and estimating statistics properties of errors in hybrid transmission. Section V states our conclusions.

II. Statistics of Error Occurrence

A. Error Occurrence Mechanism Due to Clipping

Let the frequency division multiplex (FDM) signal of AM carriers ($\boldsymbol{x}[t]$), which mainly causes the clipping in hybrid transmission, be

$$\boldsymbol{x}[t] = \sum_{i=1}^{N} m \cos[2\pi f_i t + \varphi_i] \tag{1}$$

where

m per channel OMI, which is a normalized amplitude of an AM signal;

Manuscript received December 27, 1999; revised June 21, 2000.

K. Maeda is with the Multimedia Development Center, Matsushita Electric Industrial Company, Ltd., Osaka 571-0817, Japan (e-mail: kazz@isl.mei.co.jp).

S. Komaki is with the Department of Communication Engineering, Facility of Engineering, Osaka University, Suita-shi 565-0871, Japan (e-mail: komaki@ieee.org).

Publisher Item Identifier S 0733-8724(00)09110-6.

N number of AM channels;
f_i carrier frequencies of the AM signals;
φ_i initial phases of these carriers.

In hybrid transmission, the frequency of each carrier is allocated at fixed spacing ($f_d = 6$ MHz) but with frequency offset (ε_i) due to setting error and phase noise ($\xi_i[t]$) caused by stabilities of the oscillators. Therefore, assuming the lowest carrier frequency of f_0, $\boldsymbol{x}[t]$ is given as

$$\boldsymbol{x}[t] = \sum_{i=1}^{N} m \cos\left[2\pi(f_0 + f_d(i-1) + \varepsilon_i)t + \xi_i[t] + \varphi_i\right] \tag{2}$$

and considering an envelope of $x[t]$, the form of the envelope is given as

$$\begin{aligned}\boldsymbol{R}[t] = \frac{N}{2}m^2 + \frac{N}{2}m^2 \sum_{i=1}^{N}\sum_{j=1}^{N} & \times \cos\left[2\pi\{f_d(i-j) + (\varepsilon_i - \varepsilon_j)\}t\right. \\ & \left. + (\xi_i[t] - \xi_j[t]) + (\varphi_i - \varphi_j)\right] \quad (i \neq j)\end{aligned} \tag{3}$$

As seen in (3), the form of the envelope ($\boldsymbol{R}[t]$) is mainly determined by frequency spacing and the phases of AM carriers. If we could neglect the effect of the frequency offset and the phase noise, the envelope would be determined by frequency spacing (f_d) and the initial phases (φ_i). Then a set of relationships among the phases of each carrier would not be changed and the waveform of the FDM signal would also be fixed with a certain periodicy. Fig. 1 illustrates the waveform of the FDM signal of 60 carriers of 4%/channel OMI with random phase and 40 and 60 agreed carriers' phases. As shown in Fig. 1, when the phases are random, the amplitude is randomly changed, but we cannot find an extremely large amplitude that exceeds the clipping level. On the other hand, with increasing number of agreed phases, the fragment of the amplitude exceeds the clipping level, the other portion has small levels, and the amplitude in the time domain clearly shows an amplitude peak with a period of $T_s = 167$ ns (1/6 MHz), which is equivalent to the channel spacing as seen in (3).

In an actual system, however, the relationship among the phases of each carrier gradually varies depending on each carrier's frequency offset and its stabilities. Then some of these phases occasionally coincide with each other, the envelope form also changes, and all cases in Fig. 1 can be observed. The probability appearing in the waveforms in Fig. 1 (b) and (c) is extremely low, but once the relationships of phases fall into such conditions, they stay in them much longer than the 64-QAM symbol time, and the errors occur in bursts. If we consider the envelope of (3) to evaluate the property of the clipping, it will be given as

$$\begin{aligned}A[t] = \frac{N^2}{4}m^4 + \frac{N^2}{4}m^4 \sum_{i=1}^{N}\sum_{j=1}^{N}\sum_{k=1}^{N}\sum_{l=1}^{N} & \times \cos[2\pi(\varepsilon_i - \varepsilon_j + \varepsilon_k - \varepsilon_l)t \\ & + (\xi_i[t] - \xi_j[t] + \xi_k[t] - \xi_l[t]) \\ & + (\varphi_i - \varphi_j + \varphi_k - \varphi_l)] \\ & (i \neq j, k \neq l).\end{aligned} \tag{4}$$

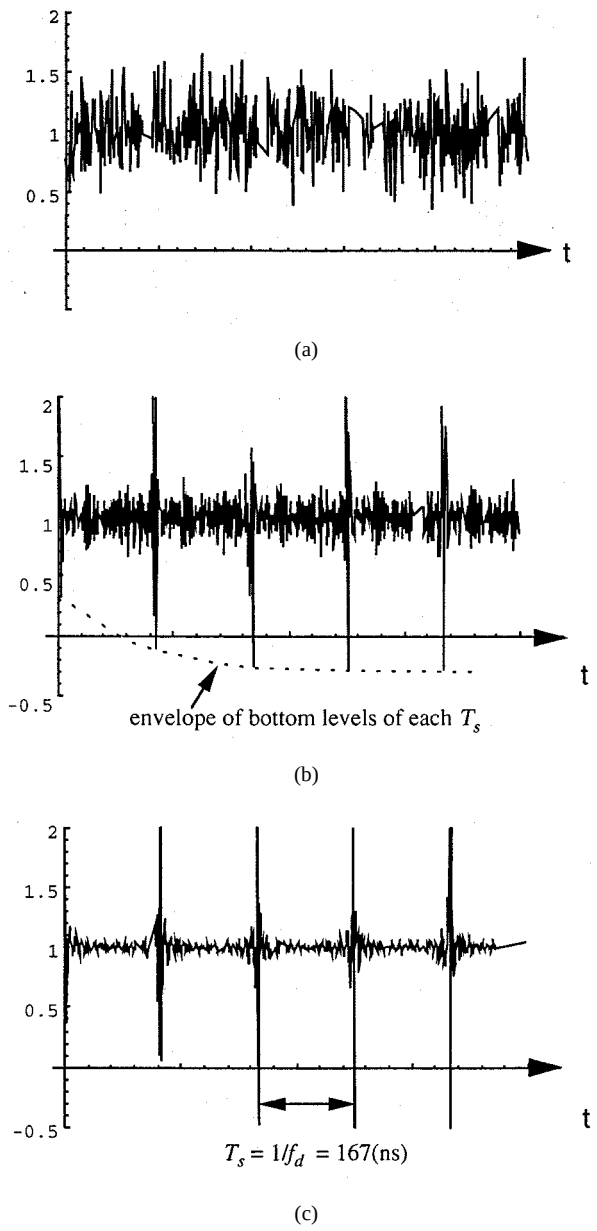

Fig. 1. Waveforms of FDM signal.

This gives the property of fluctuation of the peak level's envelope. As seen in (4), the bandwidth of the peak level's envelope depends on the offset-frequencies and the frequency stabilities. In actual application, the offset frequencies are much larger than the frequency stabilities when taking into account the specifications of CATV systems; therefore, the offset frequencies strongly dominate the bandwidth. Furthermore, a set of two different offset frequencies determines the bandwidth as seen in (4), so the bandwidth of a composite second-order distortion (CSO), composed from sets of two carrier frequencies, becomes a good reference for estimating the bandwidth. This will be discussed again in Section IV.

B. Model of Error Occurrence

The error occurrence due to impulse noise behaves according to the abovementioned mechanism. We employ a probability that it appears more than n_e error bytes in a block of the error

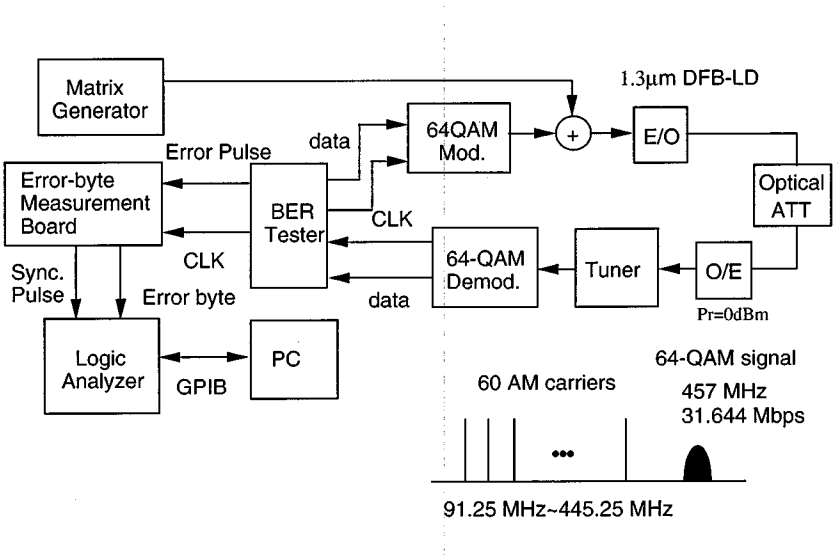

Fig. 2. Test setup for error statistics measurement.

correction code, which may be denoted by $F_i[n_e]$ or the formula of error statistics for impulse noise. At first, considering the amplitude distribution of the envelope of the FDM signal in hybrid transmission to obtain $F_i[n_e]$, it is well known that the amplitude distribution of the FDM signal $(\boldsymbol{x}[t])$ is Gaussian. Accordingly, we can easily conclude that its envelope $(\boldsymbol{R}[t])$ will be Rayleigh distributions [5], [6]. The clipping occurs when the minimum level in lower side envelope of the FDM signal stays below the threshold level of the laser diode shown in Fig. 1. Here, we assume that the envelope of peak levels of the FDM signal in each $T_s(\boldsymbol{A}[t])$ will also be Rayleigh distributions. The discussion of the duration of the clipping is the same as that for duration of the level of $\boldsymbol{A}[t]$ remaining above R. This will be obtained by using the analogy of the distribution of fading duration given in the classic paper by Rice [10]. In hybrid transmission, the OMI is the normalized carrier level, and the clipped level is $R = 1$, which is much larger than the averaged level of the FDM signal. Then, the probability that the envelope will remain above 1 for more than τ seconds can be denoted by $F_i[u]$, which is given by [8, eq. (22)]

$$F_i[u] = \exp[-u] \tag{5}$$

$$u = \frac{\tau}{\bar{t}} \tag{6}$$

$\bar{t}$ is the averaged duration that the envelope of the FDM signal remains at the clipping level and is given by

$$\bar{t} = \frac{\mu}{\sqrt{2\pi}\sigma} \tag{7}$$

where σ is a half bandwidth of $\boldsymbol{A}[t]$. μ is a normalized averaged amplitude of the FDM signal and is given by

$$\mu = m\sqrt{\frac{N}{2}}. \tag{8}$$

In [8], (5) gives the probability that the envelope stays below a level for more than τ seconds and is obtained from [8, eq. (86)]. The probability that the envelope stays above a level is derived from an equation that reverses the order of integration in (86); therefore, the results will be the same, and (5) also gives the probability that the envelope is stays above a level for more than τ seconds. τ is given as follows by using n_e:

$$\tau = n_e t_b \tag{9}$$

where t_b is a time length of the byte.

$F_i[u]$ will roughly stand for $F_i[n_e]$. Substitute τ for (9),

$$F_i[n_e] = \exp\left(-\frac{n_e t_b}{\bar{t}}\right) \tag{10}$$

III. Measurement Results

A. Test Setup

Fig. 2 shows the test setup for error occurrence measurement. Sixty AM carriers are allocated from 91.25 to 445.25 MHz with 6 MHz spacing, and the 64-QAM signal at 475 MHz is multiplexed. This FDM signal is converted to an intensity modulated optical signal at an E/O that employs a 1.3 μm distributed feedback laser diode (DFB-LD). An optical variable attenuator is used for setting received optical power. In an O/E, a p-i-n photodiode (PD) is employed to convert the optical signal back to an electrical signal. The 64-QAM signal is selected and down-converted to an IF signal of 57.0 MHz at a tuner, and the IF signal is demodulated to serial pseudonoise (PN) data of 31.6 Mb/s. This PN data is put into the BER tester. The BER tester puts out error pulses that mark error bits with clock to the error byte measurement board. The error byte measurement board counts the number of error bytes (n_e) in each error correction block of 204 bytes that coincides with the block length of the error correction in DAVIC and outputs the count results to the logic analyzer, which can store them for 16 000 blocks. The count results are sent to the computer through a general purpose interface bus (GPIB) interface. This operation was performed over several times, and then the computer counted the number of blocks (n_a) for each n_e in more than a million count results.

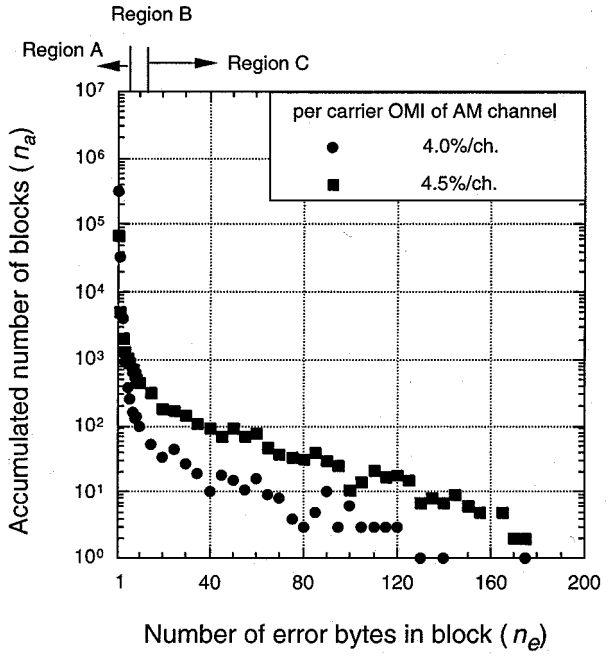

Fig. 3. Relationship between accumulated number of the blocks (n_a) and error byte count (n_e) BER of about 10^{-4}, total number of sample blocks = about 3 000 000.

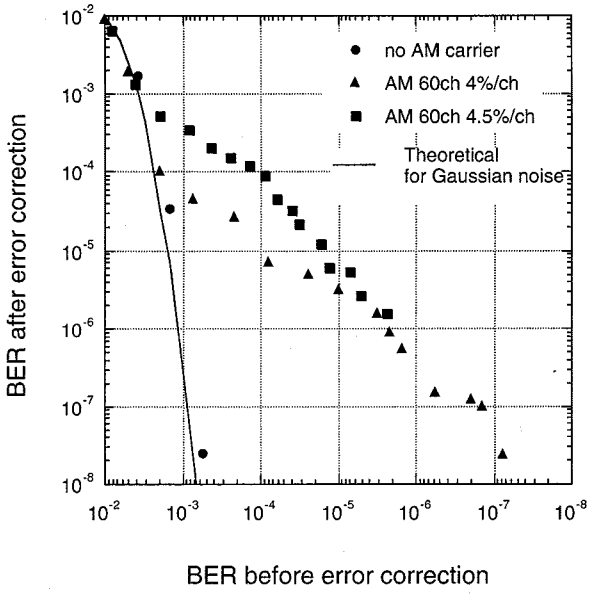

Fig. 4. Error correction performance in hybrid transmission.

B. Measurement Results

Here we give the results of measuring the number of blocks (n_a) that each have the error byte count (n_e) mentioned above for hybrid transmission, where the AM carriers have per channel OMI's (m) of 4.0% and 4.5% and the BER of the 64-QAM signals at measurement is about 10^{-4}. Fig. 3 shows measurement results of the relationship between the number of blocks and the number of error bytes. As seen in Fig. 3, the blocks having large n_e appear in considerably large numbers, even if BER reaches the 10^{-4} level. In this measurement, clipping occurred, and impulse noise surely degrades the BER, taking into account the amplitude of each carrier and the channel number. Thus, these features indicate that the errors due to impulse noise strongly show burst behaviors. The error correction cannot completely correct the error bytes if more than 96 error bytes appear in the block because such a large number of error bytes exceeds the effective interleaver block length. Blocks having such error byte counts appear at a considerably high rate. Consequently, errors due to impulse noise cannot be completely corrected by using the error correction and remain in the error correction output, as shown in Fig. 4.

The errors in hybrid transmission occur due to two independent factors: one is Gaussian noise mainly due to the thermal noise at a preamplifier in the O/E and shot noise at the laser diode in the E/O, and the other is the clipping induced impulse noise. Therefore, we believe that error occurrence can be divided into three regions. The errors due to Gaussian noise are random, and the blocks having n_e of less than five are mainly caused by Gaussian noise (region A in Fig. 3). These errors occur randomly, so the n_a rapidly decreases with increasing n_e. In region C, on the other hand, the blocks having n_e of more than

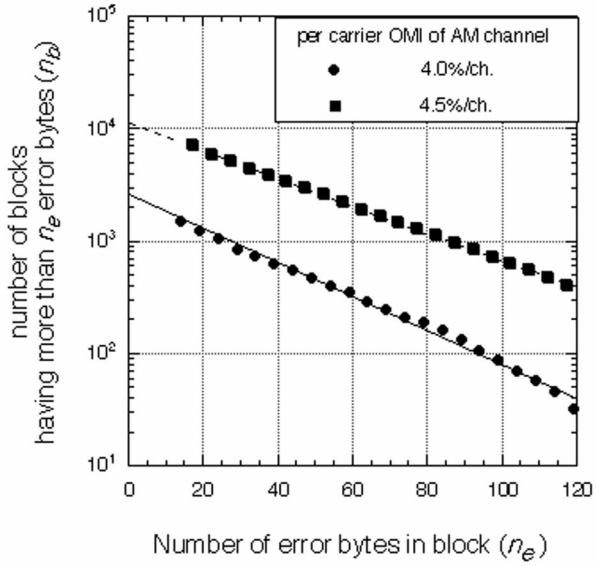

Fig. 5. Numbers of the blocks of more than $n_e(n_b)$ vs. the error byte count (n_e) for $n_e > 15$ Calculating by using data in the Fig. 3 of $n_e > 15$.

15 are due to errors caused by impulse noise; this is because the impulse noise determines the burst manner of the error occurrence. Finally, region B, having error counts from 5 to 15, is influenced by both factors.

This paper is only concerned with the influences of impulse noise on error statistics, so we did not pursue the manners of the block numbers (n_a) where $n_e \leq 15$. Instead, we calculated the relationship between the number of blocks having more than n_e error bytes (n_b) and the number of error bytes by using data in Fig. 3 for $n_e > 15$. The results of these calculations are shown in Fig. 5, which shows that the n_b values for $n_e > 15$ were plotted completely on straight lines. We believe this can be explained by using the error occurrence model described in Section II, and this result is discussed in the following section.

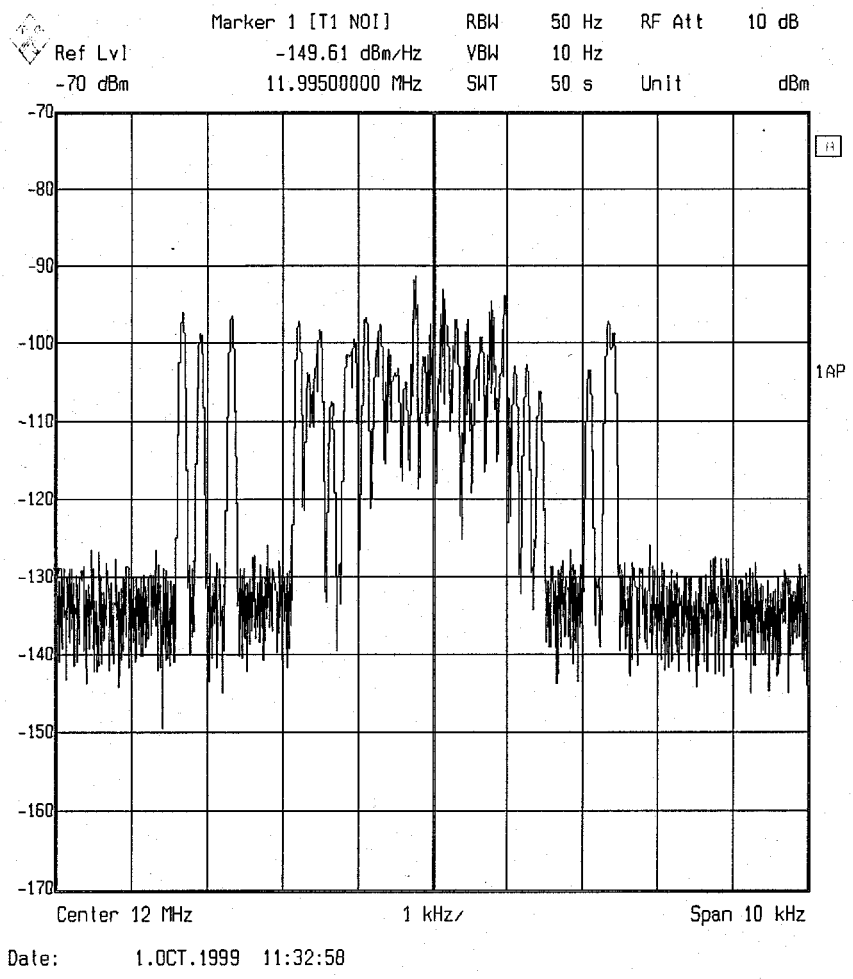

Fig. 6. Spectrum of CSO of 12 MHz setting to high-resolution bandwidth.

IV. Analysis and Discussion

A. Estimation of σ: A Bandwidth of $\boldsymbol{A}[t]$

Let us estimate σ (a bandwidth of $\boldsymbol{A}[t]$) before discussing the error statistics because it is a key parameter for determining the error statistics. σ is mainly obtained from the combination of the frequency setting errors of four carriers, as shown in (4). However, it is difficult to measure the frequency setting errors of all carriers from the matrix generator, so for estimating σ we use a composite second-order distortion (CSO) from the matrix generator, that is, carrier mixing with second-order intermodulation distortion (IM2) of distortion products of the form $f_i - f_j$. Fig. 6 shows that the CSO consists of tones that indicate the spectrum of CSO at a frequency of 12 MHz measured at high resolution on a spectrum analyzer. This CSO is carrier mixing with IM2 of the form $|f_i - f_j| = 12$ MHz; consequently, the spreading of the tones' frequencies is given by the frequency setting errors of sets of two carrier frequencies $(e_i - e_j)$. On the other hand, as the bandwidth of $\boldsymbol{A}[t]$ is obtained from $e_i - e_j + e_k - e_l$, σ can be roughly estimated by using the tone frequency spreading of the CSO. The tone frequency spreading is about 6.0 kHz by referring to the CSO spectrum of Fig. 6. σ will be twice this frequency because it is the summation of two frequency errors as described above. Therefore, σ will be about 12.0 kHz in this case.

B. Statistics of Error Occurrence

We calculated the statistics of error occurrence $(F_i[n_e])$ due to clipping by using the data shown in Fig. 5. The number of blocks for all n_e needs to be used in this calculation, but the number of blocks where $n_e < 15$ in Fig. 5 cannot be employed because they are not pure errors due to clipping. For calculating $F_i[n_e]$, we used an estimated numbers of blocks for $n_e < 15$ by assuming that they are completely on the lines in Fig. 5. The calculated results are shown in Fig. 7, where ● indicates $F_i[n_e]$ for m of 4.0%. and ■ that for 4.5%. On the other hand, we assumed that $F_i[n_e]$ is theoretically given by (10) as described in Section II. Therefore, the theoretical value calculated by using (10) with the value of σ (12.0 kHz) described above is superimposed in Fig. 7 with a solid line for m of 4.0% and a dashed line for m of 4.5%.

As shown in Fig. 7, the results of the measurement give good agreement with the values that were obtained by theoretical calculation with (10). This indicates that the assumed burst error occurrence mechanism and its analysis model, which applies

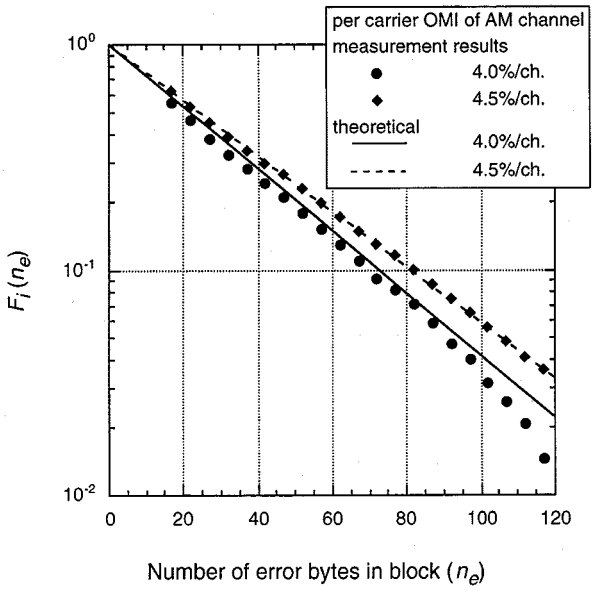

Fig. 7. Error occurrence statistics of errors due to impulse noise.

Rice's fading duration distribution model, is suitable for a model of error occurrence due to clipping. The error burst duration for the clipping error depends on the value of the total root-mean-square (rms) OMI (μ) of hybrid transmission. We experimentally confirmed this error burst property in hybrid transmission through BER measurements. We can verify it with not only the error burst measurement results, but also the theoretical calculations in this study. The error burst duration also depends on the value of σ given by the frequency setting errors. The bandwidth of each carrier of an actual system is much wider than that employed in this measurement because it is amplitude-modulated and has an audio subcarrier with FM modulation. Consequently, this will contribute to widening σ, and error durations will be much shorter than for the carriers. Also, error correction will work more effectively. We will evaluate the BER in actual systems to verify this hypothesis.

V. Conclusion

In this paper, we have presented the performance of error correction of DAVIC and the statistics of error occurrence in hybrid transmission. This error correction is ineffective for errors due to impulse noise even if the BER reaches the 10^{-4} level or lower because errors occurring under impulse noise conditions show a strong burst behavior that exceeds an effective interleaving depth. We confirmed that this burst error can be explained by behaviors of the maximum-level fluctuation of the multiplexed carrier's envelope, and demonstrated that the fading duration distribution model by Rice can be usefully applied to analyze the error occurrence properties through a comparison between the analysis results and experimental data. These evaluations are for errors of the experiment using the FDM signal with nonmodulation carriers instead of the actual modulation signals. Consequently, the results are very pessimistic and provide a very negative impact on link performance. If we design link parameters and an error correction method in accordance with these results, the setting window of link parameters would be considerably shrunk and the error correction method would be drastically changed. In practical CATV systems, however, each AM carrier is modulated by the video signal, so the spectrum of the signal is broader than that of the carrier. In our paper clipping duration could be estimated by using a bandwidth of CSO that is composed from sets of two carrier frequencies. When assuming modulation signals, their spectra are widened compared with the carrier and the bandwidth CSO by these signals is much wider than that by the carriers. Consequently, the series of clipping will be much shorter and randomized in a practical system. For such errors, performance of error correction will be more effective, and this will have a good impact on link performance. Therefore, we will continue to carefully study and clarify the error occurrence statistics to determine the optimum link parameters in practical hybrid transmission.

References

[1] K. Maeda, H. Nakata, and K. Fujito, "Analysis of BER of 16-QAM signal in AM/16-QAM hybrid optical transmission system," *Electron Lett.*, vol. 29, no. 7, pp. 640–641, Apr. 1993.

[2] X. Lu, G. E. Bodeep, and T. E. Darcie, "Clipping-induced impulse noise and its effect on bit-error performance in AM-VSB/64QAM hybrid lightwave systems," *IEEE Photon. Technol. Lett.*, vol. 6, pp. 866–868, July 1994.

[3] *Lower Layer Protocols and Physical Interfaces*, DAVIC 1.0 Specification Part 08, Jan. 1996, pp. 87–99.

[4] K. Maeda, K. Utsumi, and K. Fujito, "Error statistics of QAM channel in AM/QAM hybrid optical transmission," *IEEE Photon. Technol. Lett.*, vol. 8, pp. 1403–1405, Oct. 1996.

[5] J. E. Mazo, "Asymptotic distortion spectrum of clipped, dc-biased, Gaussian noise," *IEEE Trans. Commun.*, vol. 40, pp. 1339–1344, Aug. 1992.

[6] Q. Pan and R. J. Green, "Amplitude density of infrequent clipping impulse noise and bit-error rate impairment in AM-VSB/M-QAM hybrid lightwave systems," *IEEE Trans. Commun.*, vol. 44, pp. 1329–1334, Oct. 1996.

[7] K. Maeda and S. Morikura, "Study of BER of 64-QAM signal and OMI-window of feasible operation in analog/digital hybrid SCM transmission," *J. Lightwave Technol.*, vol. 17, pp. 1011–1017, June 1999.

[8] K. Maeda, K. Utsumi, and K. Fujito, "Transmission quality and error statistics of 64-QAM in AM/64QAM hybrid optical transmission," in *Proc. Tech. Paper 8th Conf. Optical Access Network*, Mar. 1997.

[9] S. Ovadia, "The effect of interleaver depth and QAM channel frequency offset on the performance of multichannel AM-VSB/256-QAM video transmission systems," *IEEE Photon. Technol. Lett.*, vol. 10, pp. 1174–1176, Aug. 1998.

[10] S. O. Rice, "Distribution of the duration of fades in radio transmission," *Bell Syst. Tech. J.*, vol. 37, pp. 581–635, May 1958.

Kazuki Maeda (M'96) received the B.S. degree in electrical engineering from Kobe University, Japan, in 1984.

In 1984, he joined Toshiba Corporation, Japan, and then Matsushita Electric Industrial Company, Ltd., Japan, in 1990. Since then, he has been engaged in research and development of optical communications systems by using a digital modulation method. He is currently a Senior Staff Engineer at the Multimedia Development Center of Matsushita Electric Industrial Company, Ltd., Japan.

Mr. Maeda is a member of the Institute of Electronics, Information and Communication Engineers (IEICE) of Japan.

Shozo Komaki (M'84–SM'94) was born in Osaka, Japan, in 1947. He received the B.E., M.E., and Ph.D. degrees in electrical communication engineering from Osaka University, Japan, in 1970, 1972, and 1983 respectively.

In 1972, he joined the NTT Radio Communication Laboratories, where he was engaged in repeater development for a 20-GHz digital radio system, 16-QAM, and 256-QAM systems. In 1990, he moved to Osaka University, Faculty of Engineering, and engaged in the research on radio and optical communication systems. He is currently a Professor at Osaka University.

Dr. Komaki is a member of the Institute of Electronics and Information Communication Engineers (IEICE) of Japan and the Institute of Television Engineers (ITE) of Japan. He was awarded the Paper Award and the Achievement Award from the IEICE in 1977 and 1994, respectively.